ATBD for EUMETSAT Operational GSICS Inter-Calibration of Meteosat-IASI

Doc.No. : EUM/TSS/TEN/15/803179
Issue : v1B e-signed
Date : 3 February 2016
WBS :

EUMETSAT
Eumetsat-Allee 1, D-64295 Darmstadt, Germany
Tel: +49 6151 807-7
Fax: +49 6151 807 555
http://www.eumetsat.int

This page intentionally left blank.

Document Change Record

Issue / Revision	*Date*	*DCN. No*	*Summary of Changes*
v1	14 April 2014		Original based on Pre-Operation ATBD for Meteosat-IASI EUM/MET/TEN/11/0268, updated: • Uncertainties of GSICS Correction coefficients inflated by a factor of 2, as recommended in Hewison [2013] in §6.2.4 • Clarify case of outage >14d should only reset smoothing for significant changes in §6.4
v1A	8 December 2015		First published version. Minor revision to address feedback received from GSICS Product Acceptance Team
v1B	3 February 2016		Corrected references to equation numbers

Table of Contents

Table of Figures

1 INTRODUCTION

The Global Space-based Inter-Calibration System (GSICS) aims to inter-calibrate a diverse range of satellite instruments to produce corrections ensuring their data are consistent, allowing them to be used to produce globally homogeneous products for environmental monitoring. Although these instruments operate on different technologies for different applications, their inter-calibration can be based on common principles: Observations are collocated, transformed, compared and analysed to produce calibration correction functions, transforming the observations to common references. To ensure the maximum consistency and traceability, it is desirable to base all the inter-calibration algorithms on common principles, following a hierarchical approach, described here.

This algorithm is defined as a series of generic *steps*:

1) Subsetting
2) Collocating
3) Transforming
4) Filtering
5) Monitoring
6) Correcting

Each step comprises a number of discrete components, outlined in the contents.

Each component can be defined in a hierarchical way, starting from purposes, which apply to all inter-calibrations, building up to implementation details for specific instrument pairs:

i. Describe the purpose of each component in this generic data flow.
ii. Provide different options for how these may be implemented in general.
iii. Recommend procedures for the inter-calibration class (e.g. GEO-LEO).
iv. Provide specific details for each instrument pair (e.g. SEVIRI-IASI).

The implementation of the algorithm need only follow the overall logic – so the components need not be executed strictly sequentially. For example, some parts may be performed iteratively, or multiple components may be combined within a single loop in the code.

1.1 EUMETSAT's Meteosat-IASI Inter-Calibration Algorithm

This document forms the Algorithm Theoretical Basis Document (ATBD) for the inter-calibration of the infrared channels of SEVIRI on the Geostationary (GEO) Meteosat Second Generation and MVIRI on Meteosat First Generation satellites with the Infrared Atmospheric Sounding Interferometer (IASI) on board LEO Metop satellites. This document refers to the version submitted as a candidate *Operational* GSICS product, provisionally denoted as operational/v1.0.0. The version is defined in the *processing_level* global attribute of the product's netCDF file. Changes from previous versions will be detailed in the User Guide [EUMETSAT, 2015]. .

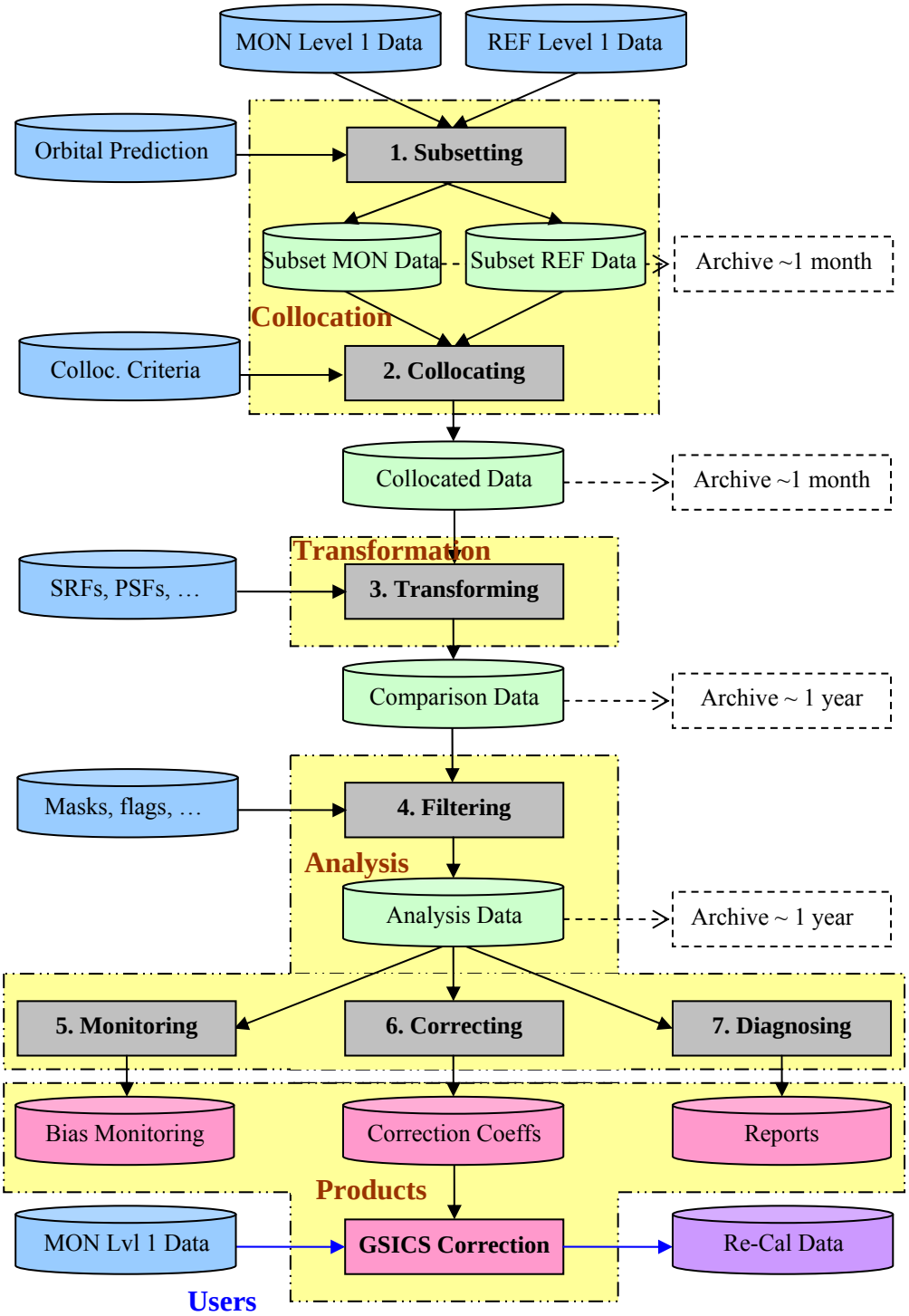

Figure 1: Diagram of generic data flow for inter-calibration of monitored (MON) instrument with respect to reference (REF) instrument

2 SUBSETTING

Acquisition of raw satellite data is obviously a critical first step in an inter-calibration method based on comparing collocated observations. To facilitate the acquisition of data for the purpose of inter-comparison of satellite instruments, prediction of the time and location of collocation events is also important.

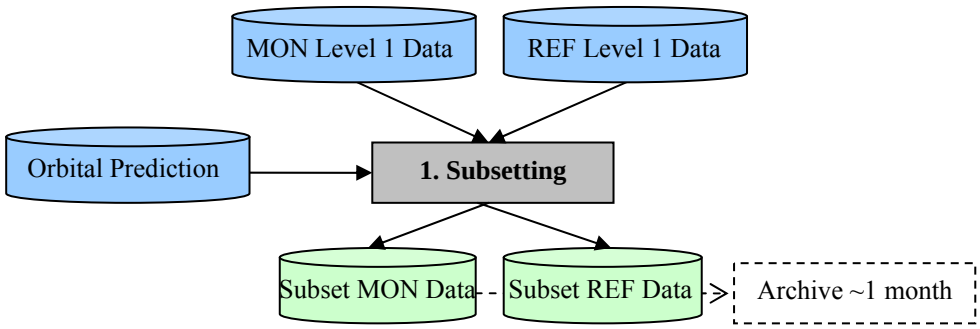

Figure 2: Step 1 of Generic Data Flow, showing inputs and outputs. MON refers to the monitored instrument. REF refers to the reference instrument.

2.1 Select Orbit

2.1.1 Purpose

We first perform a rough cut to reduce the data volume and only include relevant portions of the dataset (channels, area, time, viewing geometry). The purpose is to select portions of data collected by the two instruments that are likely to produce collocations. This is desirable because typically less than 0.1% of measurements are collocated. The processing time is reduced substantially by excluding measurements unlikely to produce collocations.

Data is selected on a per-orbit or per-image basis. To do this, we need to know how often to do inter-calibration – which is based on the observed rate of change and must be defined iteratively with the results of the inter-calibration process (see 6.6).

2.1.2 General Options

The simplest, but inefficient approach is "trial-and-error", i.e., compare the time and location of all pairs of files within a given time window.

2.1.3 Infrared GEO-LEO inter-satellite/inter-sensor Class

For inter-calibrations between geostationary and sun-synchronous satellites, the orbits provide collocations near the GEO Sub-Satellite Point (SSP) within fixed time windows every day and night. In this case, we adopt the simple approach outlined above.

We define the GEO Field of Regard (FoR) as an area close to the GEO Sub-Satellite Point (SSP), which is viewed by the GEO sensor with a zenith angle less than a threshold. Wu [2009] defined a threshold angular distance from nadir of less than 60° based on geometric considerations, which is the maximum incidence angle of most LEO sounders. This corresponds to ≈ ±52° in latitude and longitude from the GEO SSP. The GEO and LEO data is then subset to only include observations within this FoR within each inter-calibration period.

Mathematically, the GEO FoR is the collection of locations whose arc angle (angular distance) to nadir is less than a threshold or, equivalently, the cosine of this angle is larger than **min_cos_arc**. We chose the threshold **min_cos_arc = 0.5**, i.e., angular distance less than **60 degree**.

Computationally, with known Earth coordinates of GEO nadir G (0, geo_nad_lon) and granule centre P (gra_ctr_lat, gra_ctr_lon) and approximating the Earth as being spherical, the arc angle between a LEO pixel and LEO nadir can be computed with cosine theorem for a right angle on a sphere (see Figure 3):

Equation 1: $$\cos(GP) = \cos(gra\_ctr\_lat)\cos(geo\_nad\_lon - gra\_ctr\_lon)$$

If the LEO pixel is outside of GEO FoR, no collocation is considered possible. Note the arc angle GP on the left panel of Figure 3, which is the same as the angle $\angle GOP$ on the right panel, is smaller than the angle $\angle SPZ$ (right panel), the zenith angle of GEO from the pixel. This means that the instrument zenith angle is always less than 60 degrees for all collocations.

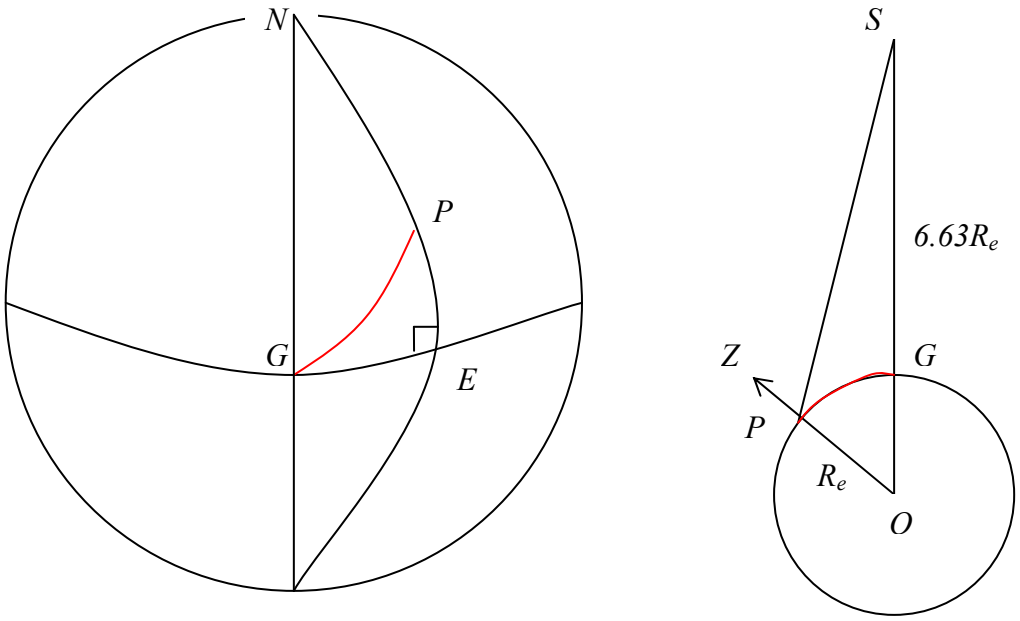

Figure 3: Computing arc angle to satellite nadir and zenith angle of satellite from Earth location

2.1.4 Specifics for Operational Meteosat-IASI

For Meteosat, the GEO FoR includes all data within ±52° lat/lon of the SSP. All IASI data within this area shall be collected from every overpass each 24 h period, beginning 00:00:00 UTC. The IASI data within this overpass is then geographically subset to only include data within this smaller GEO FoR by applying time filtering. The mean observing time within each subset IASI orbit shall be extracted and stored.

The subset Meteosat images shall be extracted with equator crossing times closest to the mean observation time within each subset IASI orbit.

3 FIND COLLOCATIONS

A set of observations from a pair of instruments within a common period (e.g. 1 day) is required as input to the algorithm. The first step is to obtain these data from both instruments, select the relevant comparable portions and identify the pixels that are spatially collocated, temporally concurrent, geometrically aligned and spectrally compatible and calculate the mean and variance of these radiances.

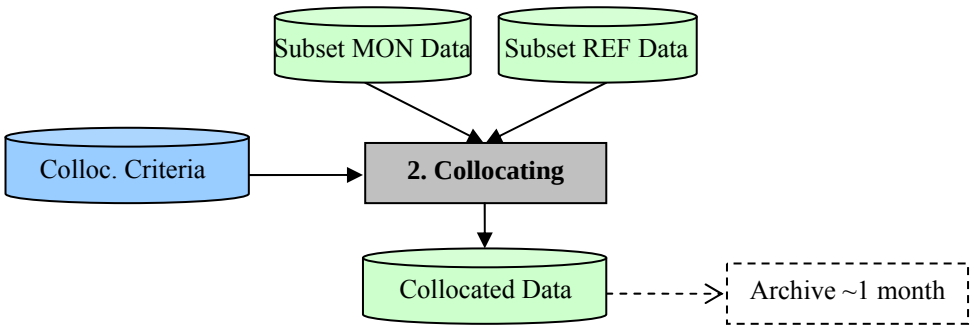

Figure 4: Step 2 of Generic Data Flow, showing inputs and outputs

3.1 Collocation in Space

3.1.1 Purpose

The following components of this step define which pixels can be used in the direct comparison. To do this, we first extract the central location of each instruments' pixels and determine which pixels can considered to be collocated, based on their centres being separated by less than a pre-determined threshold distance. At the same time we identify the pixels that define the target area (FoV) and *environment* around each collocation. These are later averaged in 4.3.

The *target area* is defined to be a little larger than the larger Field of View (FoV) of the instruments so it covers all the contributing radiation in event of small navigation errors, while being large enough to ensure reliable statistics of the variance are available. The exact ratio of the target area to the FoV will be instrument-specific, but in general will range 1 to 3 times the FoV, with a minimum of 9 'independent' pixels.

3.1.2 General Options

Where an instrument's pixels follow fixed geographic coordinates, it is possible to used a look-up table to which identify pixels match a given target's location. This is the most efficient and recommended option where available (often for geostationary instruments).

3.1.3 Infrared GEO-LEO inter-satellite/inter-sensor Class

The spatial collocation criteria is based on the nominal radius of the LEO FoV at nadir. This is taken as a threshold for the maximum distance between the centre of the LEO and GEO pixels for them to be considered spatially collocated. However, given the geometry of the already subset data, it is assumed that all LEO pixels within the GEO FoR will be within the threshold distance from a GEO pixel. The GEO pixel closest to the centre of each LEO FoV can be identified using a reverse look-up-table (e.g. using a McIDAS function).

3.1.4 Specifics for Operational Meteosat-IASI

The GEO pixel closest to the centre of each IASI iFoV is identified using a reverse look-up-table (e.g. using a McIDAS function). The IASI iFoV is defined as a circle of 12km diameter at nadir.

3.1.4.1 Specifics for Operational MVIRI-IASI

The MVIRI FoV is defined as square pixels with dimensions of 5x5km at SSP. An array of 3x3 MVIRI pixels centred on the pixel closest to centre of each IASI pixel are taken to represent the collocation target area corresponding to the IASI iFoV

3.1.4.2 Specifics for Operational SEVIRI-IASI

The SEVIRI FoV is defined as square pixels with dimensions of 3x3km at SSP. An array of 5x5 SEVIRI pixels centred on the pixel closest to centre of each IASI pixel are taken to represent the collocation target area corresponding to the IASI iFoV.

3.2 Concurrent in Time

3.2.1 Purpose

Next we need to identify which of those pixels identified in the previous step as spatially collocated are also collocated in time. Although even collocated measurements at very different times may contribute to the inter-calibration, if treated properly, the capability of processing collocated measurements is limited and the more closely concurrent ones are more valuable for the inter-calibration.

3.2.2 General Options

Each pixel identified as being spatially collocated is tested sequentially to check whether the observations from both instruments were sampled sufficiently closely in time – i.e. separated in time by no more than a specific threshold. This threshold should be chosen to allow a sufficient number of collocations, while not introducing excessive noise due to temporal variability of the target radiance relative to its spatial variability on a scale of the collocation target area – see Hewison [2009].

3.2.3 Infrared GEO-LEO inter-satellite/inter-sensor Class

The time at which each collocated pixel of the GEO image was sampled is extracted or calculated and compared to for the collocated LEO pixel. If the difference is greater than a threshold of 300s, the collocation is rejected, otherwise it is retained for further processing.

Equation 2: $|LEO\_time - GEO\_time| < \max\_\sec$, where max_sec=300s

The problem with applying a time collocation criteria in the above form is that it will often lead to only a part of the collocated pixels being analysed. As the GEO image is often climatologically asymmetric about the equator, this can lead to the collocated radiances having different distributions, which can affect the results. A possible solution to this problem is to apply the time collocation criteria to the mean times at which the collocated GEO and LEO pixels were sampled. This would ensure either all or none of the pixels within each overpass are considered to be collocated in time.

3.2.4 Specifics for Operational Meteosat-IASI

The time at which each collocated pixel of the Meteosat image was sampled is approximated by interpolating between the sensing start and end time given in the meta data, according to the scan line number. This is compared to the sample time given in the IASI Level 1c dataset.

3.2.4.1 Specifics for Operational MVIRI-IASI

The time at which each collocated pixel of the MVIRI image was sampled is approximated by interpolating between the sensing start and end time given in the meta data, according to the scan line number, which increments linearly from 1, just 'below' the South Pole to 2500, just 'above' the North Pole. If the difference is greater than a threshold of max_sec=900 s[1], the collocation is rejected, otherwise it is retained for further processing.

[1] The actual threshold applied in the prototype code is 1800 s – however, as Meteosat-7 completes a full disc scan in this period, the standard deviation of time differences of 623 s is closer to the value expected from a uniform sampling distribution within the ±900 s, so that value is used in this analysis.

3.2.4.2 Specifics for Operational SEVIRI-IASI – in Full Disk Imaging mode

SEVIRI's full disk imaging mode starts scanning from scan line 1, just 'below' the South Pole to 3712, just 'above' the North Pole in a period of 742.4 s. If the SEVIRI-IASI sampling time difference is greater than a threshold of *max_sec*=300s, the collocation is rejected, otherwise it is retained for further processing.

3.2.4.3 Specifics for Operational SEVIRI-IASI – in Rapid Scanning Service

In Rapid Scanning Service mode, SEVIRI scans only 464 lines in a period of 137.8 s, covering 15°N-70°N. If the SEVIRI-IASI sampling time difference is greater than a threshold of *max_sec*=300s, the collocation is rejected, otherwise it is retained for further processing.

3.3 Alignment in Viewing Geometry

3.3.1 Purpose

The next step is to ensure the selected collocated pixels have been observed under comparable conditions. This means they should be aligned such that they view the surface at similar incidence angles (which may include azimuth and polarisation as well as elevation angles) through similar atmospheric paths.

3.3.2 General Options

Each pixel identified as being spatially and temporally collocated is tested sequentially to check whether the viewing geometry of the observations from both instruments was sufficiently close. The criterion for zenith angle is defined in terms of atmospheric path length, according to the difference in the secant of the observations' zenith angles and the difference in azimuth angles. If these are less than pre-determined thresholds the collocated pixels can be considered to be aligned in viewing geometry and included in further analysis. Otherwise they are rejected.

3.3.3 Infrared GEO-LEO inter-satellite/inter-sensor Class

The geometric alignment of thermal infrared channels depends only on the zenith angle and not azimuth or polarisation.

Equation 3: $$\left| \frac{\cos(geo\_zen)}{\cos(leo\_zen)} - 1 \right| < \max\_zen$$

The threshold value for *max_zen* can be quite large for window channels (e.g., 0.05 for 10.8 μm channel) but must be rather small for more absorptive channels (e.g., <0.02 for 13.4 μm channel). However, unless there are particular needs to increase the sample size for window channels, a common threshold value of *max_zen*=0.01 is recommended for all channels. This results in collocations being distributed approximately symmetrically about the equator mapping out a characteristic *slanted hourglass* pattern.

Another aspect of viewing geometry alignment is azimuth angle. Similar zenith angle assures similar path length; additional requirement of similar azimuth angle assures similar line-of-sight. Line-of-sight alignment is relevant for IR spectrum in certain cases. For infrared window channels, land surface emission during daytime may be anisotropic [Minnis *et al.* 2004]. For shortwave IR band (e.g., 4 μm), azimuth angle alignment is required during daytime when solar radiation is considerable. It is, therefore recommended that inter-calibration over land and in this band are limited to night-time only cases – at the expense of limiting the dynamic range of the results.

3.3.4 Specifics for Operational Meteosat-IASI

The uncertainty analysis [EUMETSAT, 2010] suggested there would be no increase in overall uncertainty by adopting *max_zen*=0.05. However, subsequent testing of the proposed relaxation of the geometric collocation threshold [EUMETSAT, 2011] showed small, but significant, changes to the relative biases (up to 0.05 K) were produced by this change.

3.3.4.1 Specifics for Operational MVIRI-IASI

It is therefore recommended that *max_zen*=0.01 for MVIRI in full disc scanning mode, but relaxed to *max_zen*=0.05 for Rapid Scanning Service mode to increase the number of collocations.

3.3.4.2 Specifics for Operational SEVIRI-IASI – Full Disk Imaging Mode

It is therefore recommended that *max_zen*=0.01 for SEVIRI in full disk imaging mode.

Furthermore, it was found that collocations with large incidence angles can cause the regression to generate erroneous results occasionally for unknown reasons. Therefore, we limit the maximum incidence angle to 35°.

3.3.4.3 Specifics for Operational SEVIRI-IASI – Rapid Scanning Service

A relaxation of *max_zen*=0.05 is recommended for Rapid Scanning Service mode to increase the number of collocations.

Furthermore, it was found that collocations with large incidence angles can cause the regression to generate erroneous results occasionally for unknown reasons. Therefore, we limit the maximum incidence angle to 35°.

3.4 Pre-Select Channels

3.4.1 Purpose

Only broadly comparable channels from both instruments are selected to reduce data volume.

3.4.2 General Options

This selection is based on pre-determined criteria for each instrument pair.

3.4.3 Infrared GEO-LEO inter-satellite/inter-sensor Class

Only the channels of the GEO and LEO sensors are selected in the thermal infrared range of 3-15µm.

3.4.4 Specifics for Operational Meteosat-IASI

Select only the water vapour and thermal infrared channels of Meteosat.
Select all channels for IASI.

3.4.4.1 Specifics for Operational MVIRI-IASI

Select MVIRI's operational infrared and water vapour channels: "WV-1" and "IR-2".

3.4.4.2 Specifics for Operational SEVIRI-IASI

Select SEVIRI's infrared channels: 3.9, 6.2, 7.3, 8.7, 9.7, 10.8, 12.0, 13.4 µm.

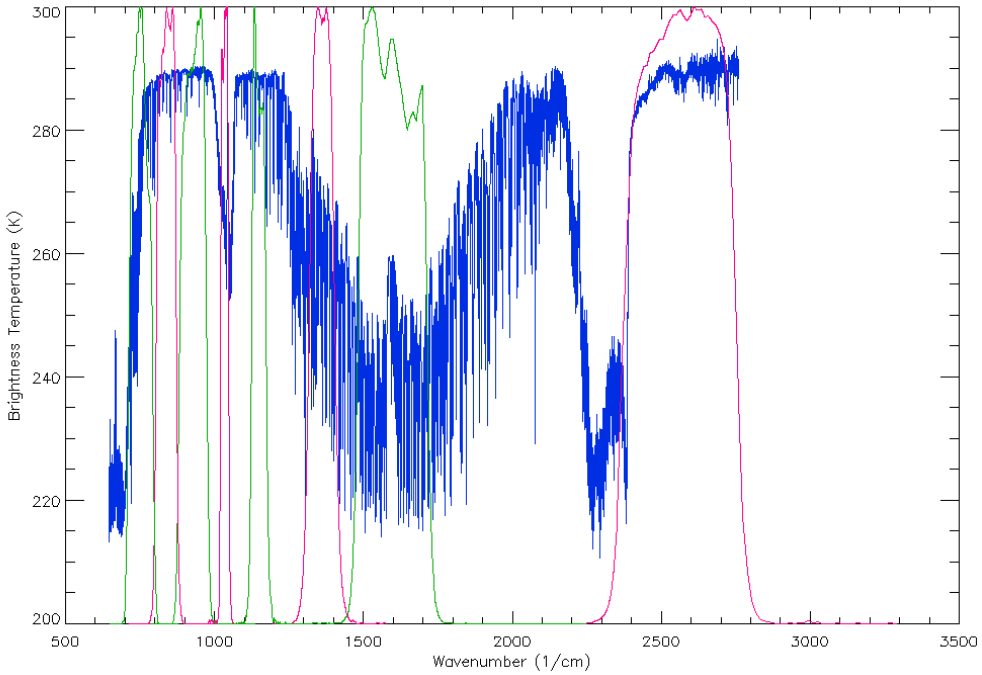

Figure 5: Example radiance spectra measured by IASI (blue), expressed in brightness temperature (K) and Spectral Response Functions of SEVIRI channels 3-11 from right to left (red/green).

3.5 Plot Collocation Map

3.5.1 Purpose

When interpreting the inter-calibration results it is often helpful to visualise the distribution of the source data used in the comparison.

3.5.2 General Options

This can be achieved by producing a map showing the distribution of collocation targets.

3.5.3 Infrared GEO-LEO inter-satellite/inter-sensor Class

The map is produced showing all the GEO-LEO pixels meeting the collocation criteria every day. These points are overlaid on a background image from an infrared window channel of the GEO instrument. This allows the distribution of cloud to be visualised and considered in the interpretation of the results.

3.5.4 Specifics for Operational Meteosat-IASI

An image is produced of radiance of the IR10.8 channel of SEVIRI or the IR channel of MVIRI over the GEO FoR on a fixed radiance scale running from 80 $mW/m^2/sr/cm^{-1}$ (white) to 140 $mW/m^2/sr/cm^{-1}$ (black). The position of the centre of all IASI iFoVs is over-plotted on this image in grey and those pixels meeting the collocation criteria are over-plotted in red, as shown in Figure 6.

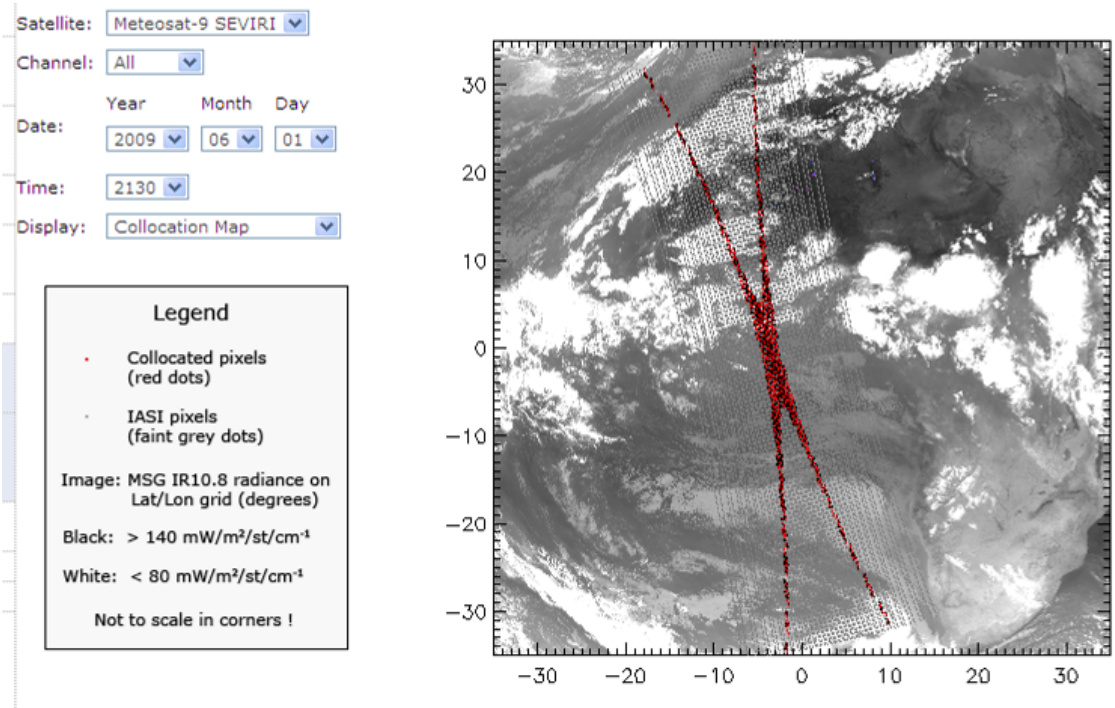

Figure 6: Example collocation map, follow inset legend.

4 TRANSFORM DATA

In this step, collocated data are transformed to allow their direct comparison. This includes modifying the spectral, temporal and spatial characteristics of the observations, which requires knowledge of the instruments' characteristics. The outputs of this step are the best estimates of the channel radiances, together with estimates of their uncertainty.

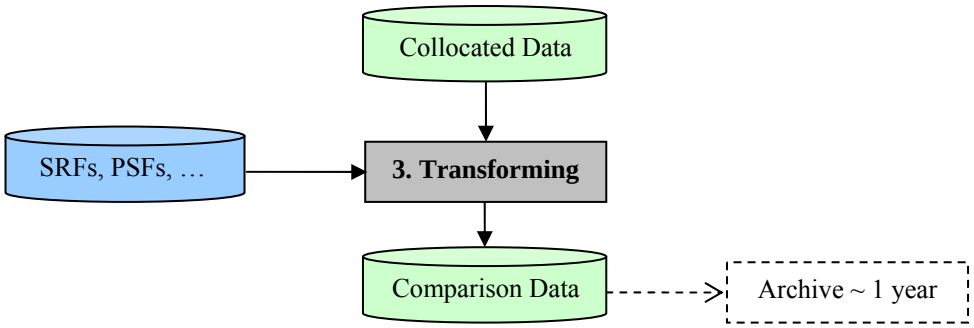

Figure 7: Step 3 of Generic Data Flow, showing inputs and outputs

4.1 Convert Radiances

4.1.1 Purpose

Convert observations from both instruments to a common definition of radiance to allow direct comparison.

4.1.2 General Options

The instruments' observations are converted from Level 1.5/1b/1c data to radiances, using pre-defined, published algorithms specific for each instrument.

4.1.3 Infrared GEO-LEO inter-satellite/inter-sensor Class

Perform comparison in radiance units: $mW/m^2/st/cm^{-1}$.

4.1.4 Specifics for Operational Meteosat-IASI

IASI data are converted to radiances using the published algorithm [EUMETSAT, 2008].

4.1.5 Specifics for Operational MVIRI-IASI

Radiances are converted to brightness temperatures following Tjemkes [2005].

4.1.6 Specifics for Operational SEVIRI-IASI

The Meteosat effective radiance definition applicable to each level 1.5 dataset, described by EUMETSAT [2012], is used, accounting for the instrument's Spectral Response Functions [EUMETSAT, 2006].

4.2 Spectral Matching

4.2.1 Purpose

Firstly, we must identify which channel sets provide sufficient common information to allow meaningful inter-calibration. These are then transformed into comparable pseudo channels, accounting for the deficiencies in channel matches.

4.2.2 General Options

The Spectral Response Functions (SRFs) must be defined for all channels. The observations of channels identified as comparable are then co-averaged using pre-determined weightings to give *pseudo channel* radiances. A Radiative Transfer Model can be used to account for any differences in the pseudo channels' characteristics. The uncertainty due to spectral mismatches is then estimated for each channel.

4.2.3 Infrared GEO-LEO inter-satellite/inter-sensor Class

For hyper-spectral instruments, all SRFs are first transformed to a common spectral grid. The LEO hyperspectral channels are then convolved with the GEO channels' SRFs to create synthetic radiances in pseudo-channels, accounting for the spectral sampling and stability in an error budget.

Equation 4: $$R_{GEO} = \frac{\int_{\nu} R_{\nu} \Phi_{\nu} d\nu}{\int_{\nu} \Phi_{\nu} d\nu}$$

where R_{GEO} is the simulated GEO radiance, R_{ν} is LEO radiance at wave number ν, and Φ_{ν} is GEO spectral response at wave number ν.

In general LEO hyperspectral sounders do not provide complete spectral coverage of the GEO channels either by design (e.g. gaps between detector bands), or by subsequent hardware failure (e.g. broken or noisy channels). The radiances in these *gap channels* shall be accounted by one of the following techniques:

Tahara and Kato [2009] define virtual channels named gap channels to fill the spectral gaps and introduce the spectral compensation method by constrained optimization. The gap channels to fill the AIRS spectral gaps (AIRS gap channels) are defined by 0.5 cm^{-1} intervals, and are characterized by a unique SRF, whose shape is a Gaussian curve with a sigma of 0.5 cm^{-1}. The gap channels to extend the IASI spectral region (IASI gap channels) are defined by the same intervals (0.25 cm^{-1}) and SRFs as the IASI level 1c channels. The radiances of the missing channels are calculated by regression analysis using radiative transfer simulated radiances with respect to the eight atmospheric model profiles as explanatory variables.

Equation 5: $$\log I_i^{calc} = c_0 + \sum_{k=1}^{K} c_k \log I_{i,k}^{sim} \left(i = hyper\ and\ gap\ channels\right),$$

where I_i^{calc} is the calculated radiance of the hyper channel i, $I_{i,k}^{sim}$ is the simulated radiance of the hyper channel i with respect to the atmospheric model profile k, $c_k\left(k = 1,\ldots,K\right)$ are regression coefficients, and K is the number of the atmospheric model profiles. Equation 5 introduces logarithm radiances as response and explanatory variables in order to increase

fitting accuracy and avoid calculation of negative radiance. The regression coefficients c_k are independent of the hyper channels, and are generated for each scan position of the hyper sounder. c_k are obtained by the least-square method applying a set of validly observed radiances I_i^{obs} in place of I_i^{calc} to Equation 5.

Equation 6: $$\{c_k\} = \arg\min \sum_{i=exist(I_i^{obs})} \left\{ \log I_i^{obs} - \left(c_0 + \sum_k c_k \log I_{i,k}^{sim} \right) \right\}^2 .$$

Once the regression coefficients c_k are computed, the radiances of the missing channels can be calculated by Equation 5. It might be possible to apply the observed radiances of all hyper channels to Equation 6 to compute c_k and then calculate the radiances of all missing channels at once. However, this yields a large fitting error in practice. In inter-calibration application, the coefficients c_k are computed for each broadband channel spectral region. Equation 5 and Equation 6 use the simulated radiances $I_{i,k}^{sim}$. For the radiance simulation, this study uses the following eight atmospheric model profiles:

1. U.S. standard without cloud,
2. U.S. standard with opaque cloud with tops at 500 hPa altitude,
3. U.S. standard with opaque cloud with tops at 200 hPa altitude,
4. Tropical without cloud,
5. Tropical with opaque cloud with tops at 500 hPa altitude,
6. Tropical with opaque cloud with tops at 200 hPa altitude,
7. Mid-latitude summer without cloud,
8. Mid-latitude winter without cloud.

These profiles include not only clear sky conditions but also cloudy conditions because Equation 5 should be applicable under any weather conditions. As for radiative transfer code, the line-by-line code LBLRTM [Clough et al., 1995] version 11.1 is used with the HITRAN2004 spectroscopy line parameter database [Rothman et al., 2003] including the AER updates version 2.0 (AER Web page). The emissivities of the surface and clouds are assumed to be one. The benefit of this spectral compensation method is that it does not require radiative transfer computation to be run in inter-calibration operation. This not only speeds up the computation but also prevents super channel radiance computation from introducing biases contained in radiative transfer code and atmospheric state fields.

4.2.4 Specifics for Operational Meteosat-IASI

IASI channels are assumed to be spectrally stable and contiguously sampled with a spectral resolution of 0.25 cm^{-1}.

4.2.4.1 Specifics for Operational MVIRI-IASI

MVIRI's SRFs for WV-1 and IR-2 channels, published by EUMETSAT [2005] are interpolated onto IASI's spectral grid in wavenumber-space using a linear interpolation. Any negative responses in the interpolated SRFs are set to zero.

4.2.4.2 Specifics for Operational SEVIRI-IASI

SEVIRI's SRFs for an operating temperature of 95K, published by EUMETSAT [2006] are interpolated onto IASI's spectral grid in wavenumber-space using a bilinear interpolation. Any negative responses in the interpolated SRFs are set to zero.

The radiance missing from IASI's coverage of SEVIRI IR3.9 channel is also estimated following the constrained optimization approach described above [Tahara and Kato, 2009], using coefficients specified therein specifically for SEVIRI-IASI. These gap channels to extend the IASI spectral region (IASI gap channels) are defined by the same intervals (0.25 cm^{-1}) and SRFs as the IASI level 1c channels.

4.3 Spatial Matching

4.3.1 Purpose

The observations from each instrument are transformed to comparable spatial scales. This involves averaging all the pixels identified in 3 as being within the *target* and *environment* areas. The uncertainty due to spatial variability is estimated.

4.3.2 General Options

The Point Spread Functions (PSFs) of each instrument are identified. The *target area* and *environment* around it were specified in 3. Now the pixels within these areas are identified and their radiances are averaged and their variance calculated to estimate the uncertainty on the average due to spatial variability, accounting for any over-sampling.

4.3.3 Infrared GEO-LEO inter-satellite/inter-sensor Class

The *target area* is defined as the nominal LEO FoV at nadir. The GEO pixels within target area are averaged using a uniform weighting and their variance calculated. The *environment* is defined by the GEO pixels within twice the radius of the target area from the centre of each LEO FoV.

4.3.4 Specifics for Operational Meteosat-IASI

As above, where the IASI iFoV is defined as a circle of 12km diameter at nadir.

4.3.4.1 Specifics for Prototype MVIRI-IASI

The MVIRI FoV is defined nominally as square pixels with lengths of 5km at SSP. These are assumed to be constant across collocation domain. The *target area* is defined by arrays of 3x3 MVIRI pixels closest to centre of each IASI iFoV, as shown in Figure 8. This is somewhat larger than the size of the IASI iFoV at nadir, but smaller at the extremes of its scan. The *environment* is defined by arrays of 5x5 MVIRI pixels on the same centre.

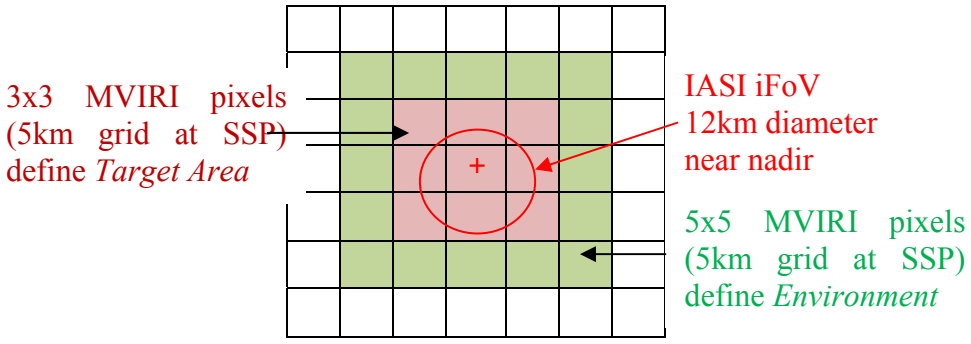

Figure 8: Definition of* Target Area *as 3x3 MVIRI pixels to spatially match an IASI iFoV.

4.3.4.2 Specifics for Prototype SEVIRI-IASI

The SEVIRI FoV is defined nominally as square pixels with lengths of 3km at SSP. These are assumed to be constant across collocation domain. The *target area* is defined by arrays of 5x5 SEVIRI pixels closest to centre of each IASI iFoV, as shown in

Figure 9. This is somewhat larger than the size of the IASI iFoV at nadir, but smaller at the extremes of its scan. The *environment* is not defined, as it is not used in further analysis.

The *environment* is defined by a array 9x9 SEVIRI pixels, centred on the IASI iFoV.

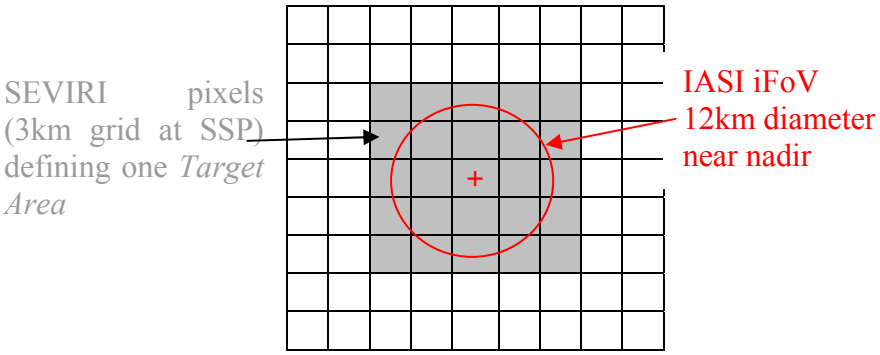

Figure 9: Definition of* Target Area *as 5x5 SEVIRI pixels to spatially match an IASI iFoV.* Environment *is defined by array of 9x9 SEVIRI pixels centred on IASI iFoV.

4.4 Viewing Geometry Matching

4.4.1 Purpose

Despite the collocation criteria described in 3.3, each instrument can measure radiance from the collocation targets in slightly different viewing geometry. It may be possible to account for small differences by considering simplified a radiative transfer model.

4.4.2 General Options

Differences in viewing geometry within the collocation criteria described in 3.3 are assumed to be negligible and ignored in further analysis. Although it may be possible to account for small differences by considering simplified a radiative transfer model, this has not been implemented at this time.

4.4.3 Infrared GEO-LEO inter-satellite/inter-sensor Class

Differences in viewing geometry within the collocation criteria described in 3.3 are assumed to be negligible and ignored in further analysis.

4.4.4 Specifics for Operational Meteosat-IASI

As above.

4.5 Temporal Matching

4.5.1 Purpose

Different instruments measure radiance from the collocation targets at different times. The impact of this difference can usually be reduced by careful selection, but not completely eliminated. The timing difference between instruments' observations is established and the uncertainty of the comparison is estimated based on (expected or observed) variability over this timescale.

4.5.2 General Options

Each instrument's sample timings are identified.

4.5.3 Infrared GEO-LEO inter-satellite/inter-sensor Class

Only the GEO image closest to the LEO equator crossing time is selected. The time difference between the collocated GEO and LEO observations is neglected and the collocation targets are assumed to be sampled simultaneously, contributing no additional uncertainty to the comparison.

4.5.4 Specifics for Operational Meteosat-IASI

As above.

5 FILTERING

The collocated and transformed data will be archived for analysis. Before that, the GSICS inter-calibration algorithm reserves the opportunity to remove certain data that should not be analyzed (quality control), and to add auxiliary data that will add further analysis. For example, it may be useful to incorporate land/sea/ice masks and/or cloud flags to better classify the results.

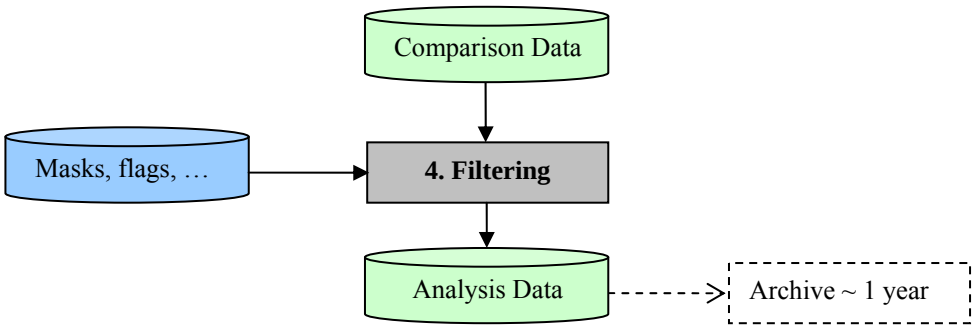

Figure 10: Step 4 of Generic Data Flow, showing inputs and outputs.

5.1 Uniformity Test

5.1.1 Purpose

Knowledge of scene uniformity is critical in reducing and evaluating inter-calibration uncertainty. To reduce uncertainty in the comparison due to spatial/temporal mismatches, the collocation dataset may be filtered so only observations in homogenous scenes are compared.

5.1.2 General Options

The approach adopted in this version is not to reject collocations based on a threshold of scene variability, but to use scene variances as weightings in the regression of collocated radiances. Comparatively, the threshold option has the theoretical disadvantage of subjectivity but practical advantage of substantially reducing the amount of data to be archived. Recent analysis [Tobin, personal communication, 2009] also indicates that the threshold option is always suboptimal compared to the weight option.

5.1.3 Infrared GEO-LEO inter-satellite/inter-sensor Class

The variance of the radiances of all the GEO pixels within each LEO FoV is calculated in 4.3.

5.1.4 Specifics for Operational Meteosat-IASI

An option is included to reject any targets where the standard deviation of the scene radiance is >5% of the standard radiance (see 4b). This is only used to clean-up the scatterplots showing the regression of collocated radiances to prevent points with large error bars (high spatial variability) dominating the plots generated in 6.2, as they have a negligible impact on the regression coefficients.

5.2 Outlier Rejection

5.2.1 Purpose

To prevent anomalous observations having undue influence on the results, 'outliers' may be identified and rejected on a statistical basis. Small number of anomalous pixels in the environment, even concentrated, may not fail the uniformity test. However, if they appear only in one sensor's field of view but not the other, it can cause unwanted bias in a single comparison.

5.2.2 General Options

The radiances in the target area are compared with those in the surrounding *environment*, and those targets which are significantly different from the environment (3σ) may be rejected.

For a normally distributed population of size *N*, mean *M*, and standard deviation *S,* the difference between a single sample and *M* has the probability of ~68% to be less than *S*, ~95% to be less than 2*S*, and so forth. Similarly, the difference between the mean of n^2 samples and *M* has the probability of ~68% to be less than $S/n[(N-n)/(N-1)]$, ~95% to be less than $2S/n[(N-n)/(N-1)]$, and so forth. This property is used to test whether the collocation area is an outlier for the otherwise uniform environment:

Equation 7: $$\left|\frac{1}{n^2}\sum_{i=1}^{n^2} R_i - M\right| \le \frac{S}{n}\frac{N-n}{N-1} Gaussian(=3)$$

where R is radiance from individual pixel, n2 is the number of samples, and Gaussian is a threshold. The probability that the rejected sample is an outlier is 68% if *Gaussian*=1, 95% if *Gaussian*=2, and more than 99% if *Gaussian*=3.

5.2.3 Infrared GEO-LEO inter-satellite/inter-sensor Class

The mean GEO radiances within each LEO FoV are compared to the mean of their *environment*. Targets where this difference is >3 times the standard deviation of the environment's radiances are rejected.

5.2.4 Specifics for Operational Meteosat-IASI

As above.

5.3 Auxiliary Datasets

5.3.1 Purpose

It may be useful to incorporate land/sea/ice masks and/or cloud flags to allow analysis of statistics in terms of other geophysical variables – e.g. land/sea/ice, cloud cover, etc.

It may also be possible to estimate the spatial variability within the LEO FoV from collocated AVHRR observations from the same LEO satellite.

5.3.2 General Options

Not yet implemented.

5.3.3 Infrared GEO-LEO inter-satellite/inter-sensor Class

Not yet implemented.

5.3.4 Specifics for Operational Meteosat-IASI

Not yet implemented.

6 MONITORING

This step includes the actual comparison of the collocated radiances produced in Steps 1-4, the production of statistics summarising the results to be used in the Correcting step, and reporting any differences in ways meaningful to a range of users.

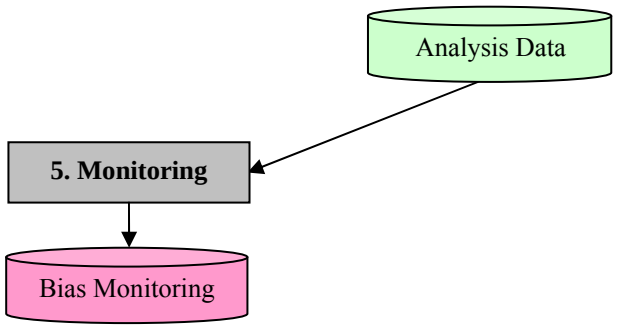

Figure 11: Step 5 of Generic Data Flow, showing inputs and outputs.

6.1 Define Standard Radiances (Offline)

6.1.1 Purpose

This component provides standard reference scene radiances at which instruments' inter-calibration bias can be directly compared and conveniently expressed in units understandable by the users. Because biases can be scene-dependent, it is necessary to define channel-specific *standard radiances*. More than one standard radiance may be needed for different applications – e.g. clear/cloudy, day/night. This component is carried out offline.

6.1.2 General Options

The standard radiances should be calculated for each channel *a priori* using a Radiative Transfer Model (RTM) based on a standard atmospheric profile and surface conditions. The reference radiance should be calculated at nadir, at night for IR channels or at a given solar angle (for vis/nir channels), in a 1976 US Standard Atmosphere, in clear skies, over the sea with a SST=+15C and wind speed (7m/s), using some standard RTM, accounting for the SRF of each channel. This has the advantages of being independent of any instrument biases and provides standard radiances against which we can compare the instruments' relative biases derived from a number of different inter-calibration techniques.

6.1.3 Infrared GEO-LEO inter-satellite/inter-sensor Class

A above.

6.1.4 Specifics for Operational Meteosat-IASI

As above.

6.1.5 Specifics for Prototype MVIRI-IASI

The calculation of standard radiances is implemented directly, using RTTOV-9, giving the following results for the IR channels MVIRI on both Meteosat-7:

Channel	WV	IR
T_{bstd} (K)	237	285

6.1.5.1 Specifics for Operational SEVIRI-IASI

The calculation of standard radiances is implemented directly, using RTTOV-9, giving the following results for the IR channels SEVIRI on all Meteosat Second Generation satellites:

Ch (μm)	3.9	6.2	7.3	8.7	9.7	10.8	12.0	13.4
T_{bstd} (K)	284	236	255	284	261	286	285	267

6.2 Regression of Most Recent Results

6.2.1 Purpose

Regression is used as the basis of the systematic comparison of collocated radiances from two instruments. (This comparison may also be done in counts or brightness temperature.) Regression coefficients shall be made available to users to apply the GSICS Correction to the monitored instrument, re-calibrating its radiances to be consistent with those of the reference instrument. Scatterplots of the regression data should also be produced to allow visualisation of the distribution of radiances.

Regressions also allow us to investigate how biases depend on various geophysical variables and provides statistics of any significant dependences, which can used to refine corrections and allows investigation of the possible causes. Such investigations should be carried out offline and may result in future refinements to the ATBD.

6.2.2 General Options

The recommended approach is to perform a weighted linear regression of collocated radiances. The inverse of the sum of the spatial and temporal variance of the target radiance and the radiometric noise provide an estimated uncertainty on each dependent point, which is used as a weighting. (Including the radiometric noise ensures that very homogeneous targets scenes where all the pixels give the same radiance do not have undue influence on the weighted regression.)

This method produces estimates of regression coefficients describing the slope and offset of the relationship between the two instruments' radiances – together with their uncertainties, expressed as a covariance. The problem of correlation between the uncertainties on each coefficient may be reduced by performing the regression on a transformed dataset – for example, by subtracting the mean or reference radiance from each set.

The observations of the reference instrument, x, and monitored instrument, y, are fitted to a straight line model of the form:

Equation 8: $\hat{y}(x) = a + bx$

We assume an uncertainty σ_i associated with each measurement, y_i, is known and that the dependent variable, x_i is also known.

To fit the observed data to the above model, we minimise the chi-square merit function:

Equation 9: $\chi^2(a,b) = \sum_{i=1}^{N} \left(\frac{y_i - a - bx_i}{\sigma_i} \right)^2$

This can be implemented following the method described in Section 15.2 of Numerical Recipes [Press *et al.*, 1992], which is implemented in the *POLY_FIT* function of IDL, yielding the following estimates of the regression coefficients:

Equation 10: $$a = \frac{\sum_{i=1}^{N}\frac{x_i^2}{\sigma_i^2}\sum_{i=1}^{N}\frac{y_i}{\sigma_i^2} - \sum_{i=1}^{N}\frac{x_i}{\sigma_i^2}\sum_{i=1}^{N}\frac{x_i y_i}{\sigma_i^2}}{\sum_{i=1}^{N}\frac{1}{\sigma_i^2}\sum_{i=1}^{N}\frac{x_i^2}{\sigma_i^2} - \left(\sum_{i=1}^{N}\frac{x_i}{\sigma_i^2}\right)^2},$$

Equation 11: $$b = \frac{\sum_{i=1}^{N}\frac{1}{\sigma_i^2}\sum_{i=1}^{N}\frac{x_i y_i}{\sigma_i^2} - \sum_{i=1}^{N}\frac{x_i}{\sigma_i^2}\sum_{i=1}^{N}\frac{y_i}{\sigma_i^2}}{\sum_{i=1}^{N}\frac{1}{\sigma_i^2}\sum_{i=1}^{N}\frac{x_i^2}{\sigma_i^2} - \left(\sum_{i=1}^{N}\frac{x_i}{\sigma_i^2}\right)^2},$$

their uncertainties:

Equation 12: $$\sigma_a^2 = \frac{\sum_{i=1}^{N}\frac{x_i^2}{\sigma_i^2}}{\sum_{i=1}^{N}\frac{1}{\sigma_i^2}\sum_{i=1}^{N}\frac{x_i^2}{\sigma_i^2} - \left(\sum_{i=1}^{N}\frac{x_i}{\sigma_i^2}\right)^2},$$

Equation 13: $$\sigma_b^2 = \frac{\sum_{i=1}^{N}\frac{1}{\sigma_i^2}}{\sum_{i=1}^{N}\frac{1}{\sigma_i^2}\sum_{i=1}^{N}\frac{x_i^2}{\sigma_i^2} - \left(\sum_{i=1}^{N}\frac{x_i}{\sigma_i^2}\right)^2},$$

and their covariance:

Equation 14: $$\mathrm{cov}(a,b) = \frac{-\sum_{i=1}^{N}\frac{x_i}{\sigma_i^2}}{\sum_{i=1}^{N}\frac{1}{\sigma_i^2}\sum_{i=1}^{N}\frac{x_i^2}{\sigma_i^2} - \left(\sum_{i=1}^{N}\frac{x_i}{\sigma_i^2}\right)^2}.$$

6.2.3 Infrared GEO-LEO inter-satellite/inter-sensor Class

Inter-calibrations are repeated daily using only night-time LEO overpasses. Collocations are weighted by the inverse the sum of the spatial and temporal variance of target radiances and their radiometric noise level in the regression. (The inclusion of the radiometric noise ensures the weights never become infinite due to collocation targets with zero variance.) Scatterplots of the regression data should also be produced to allow visualisation of the distribution of radiances, following the example shown in Figure 12.

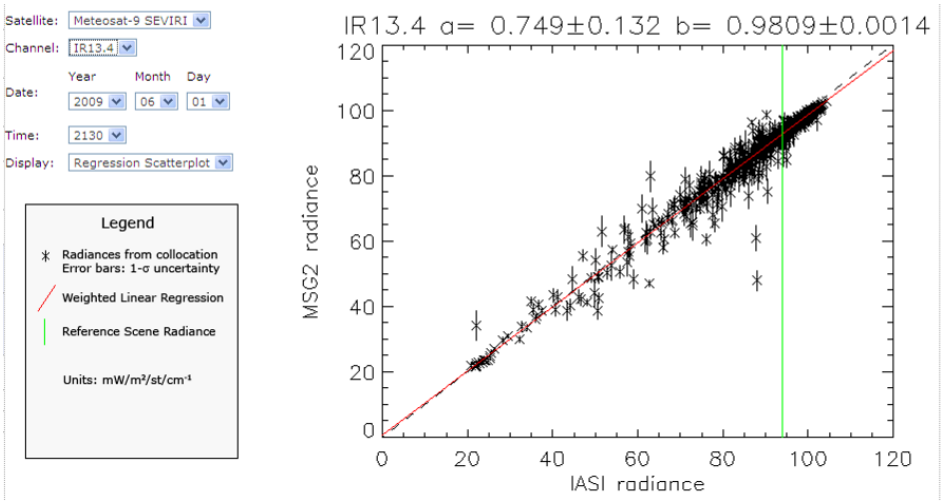

Figure 12: Example scatterplot showing regression of collocated radiances, following legend.

6.2.4 Specifics for Operational Meteosat-IASI

Implement as above. The range of incidence angles was implicitly extended to <40° by changing the FoR constraints. Inter-calibrations are attempted every day (although only ~½ of cases contain collocations).

The temporal variance is assumed to be equal to the spatial variance, so its contribution to the weighting is multiplied by √2 and added in quadrature to the radiometric noise. The radiometric noise for IASI is assumed to be negligible when averaged over all channels within the SRF of each Meteosat channel.

The uncertainties of the demonstration and pre-operational GSICS Correction coefficients were analysed by Hewison [2013] and EUMETSAT [2015], respectively. Both analyses concluded that the uncertainties were systematically underestimated by the error propagation in the weighted regression described above, and recommended inflating the coefficients' uncertainties by a factor of 2 (2^2 for the covariance). This change is implemented in the operational version of the algorithm:

Equation 15a: $\sigma_a^{'} = 2\sigma_a$,

Equation 16a: $\sigma_b^{'} = 2\sigma_b$,

Equation 17a: $\mathrm{cov}'(a,b) = 4\,\mathrm{cov}(a,b)$.

6.2.4.1 Specifics for Operational MVIRI-IASI

The radiometric noise on each pixel for the MVIRI channels is given by [Schmetz et al. 2002]:

Channel	WV	IR
Met-7 Noise [K]	0.25	0.30

6.2.4.2 Specifics for Operational SEVIRI-IASI

The radiometric noise on each pixel for the SEVIRI channels is given by [EUMETSAT, 2007] for example, for "ambient calibrations" at 95K. For MSG-3 and -4 values are taken from average noise before and after the first decontamination reported in the respective MSG System Commissioning Image Verification and Validation Reports.

Channel IR	3.9	6.2	7.3	8.7	9.7	10.8	12.0	13.4
MSG-1 Noise [K]	0.013	0.045	0.065	0.07	0.115	0.065	0.12	0.185
MSG-2 Noise [K]	0.09	0.05	0.05	0.075	0.10	0.07	0.10	0.205
MSG-3 Noise [K]	0.09	0.04	0.05	0.06	0.09	0.065	0.135	0.25
MSG-4 Noise [K]	0.10	0.06	0.04	0.06	0.10	0.06	0.09	0.21

6.3 Bias Calculation

6.3.1 Purpose

Inter-calibration biases should be directly comparable for representative scenes and conveniently expressed in units understandable by the users. Because biases can be scene-dependent, they are evaluated here at the standard radiances defined in 6.1.

6.3.2 General Options

Regression coefficients are applied to estimate expected bias, $\Delta\hat{y}(x_{STD})$, and uncertainty, $\sigma_{\hat{y}}(x_{STD})$, for standard radiances, accounting for correlation between regression coefficients.

Equation 18: $\Delta\hat{y}(x_{STD}) = a + bx_{STD} - y_{STD}$,

noting that $y_{STD} = x_{STD}$ and

Equation 19: $\sigma^2_{\hat{y}}(x_{STD}) = \sigma^2_a + \sigma^2_b x^2_{STD} + 2\,\mathrm{cov}(a,b)x_{STD}$

The results may be expressed in absolute or percentage bias in radiance, or brightness temperature differences.

6.3.3 Infrared GEO-LEO inter-satellite/inter-sensor Class

Biases and their uncertainties are converted from radiances to brightness temperatures for visualisation purposes.

6.3.4 Specifics for Operational Meteosat-IASI

The definition of effective radiance is used in the conversion to brightness temperatures [EUMETSAT, 2012].

6.4 Consistency Test

6.4.1 Purpose

The most recent results are tested for statistical consistency with the previous time series of results. Users should be alerted to any sudden changes in the calibration of the instruments, allowing them to investigate potential causes and *reset trend* statistics calculated in 6.5. The consistency test may be performed in terms of regression coefficients or biases.

6.4.2 General Options

The biases calculated for standard radiances from the most recent collocations are compared to the statistics of the biases' trends calculated in 6.5 from previous results. If the most recent result falls outside the 3-σ (99.7%) confidence limits estimated from the trend statistics, an alert should be raised. This alert should trigger the Principle Investigator to check the cause of the change and reset the trends by issuing a *trend reset*.

Equation 20: $$\left| \frac{y_i - \hat{y}_i(x_i)}{\sigma_{\hat{y}(x_i)}} \right| \geq Gaussian(=3)$$

In the case where no collocations are generated by the processing system within the given time window, no new results should be generated. When the processing is restarted after such an outage, the bias should be tested for consistency with the previous results as described above. Only in case the new results are statistically different from the results before the interruption, does an alert need to be raised to trigger the operator to investigate whether a *trend reset* needs to be issued.

6.4.3 Infrared GEO-LEO inter-satellite/inter-sensor Class

As above.

6.4.4 Specifics for Operational Meteosat-IASI

As above.

6.5 Trend Calculation

6.5.1 Purpose

It is important to establish whether an instrument's calibration is changing slowly with time. It is possible to establish this from a time-series of inter-comparisons by calculating a trend line using a linear regression with date as the independent variable. Only the portion of the time series since the most recent *trend reset* is analysed, to allow for step changes in the instruments' calibration.

6.5.2 General Options

The time series of biases evaluated at standard radiances can be regressed against the time (date) as the independent variable. The linear regression can be weighted by the calculated uncertainty on each bias. The regression coefficients including uncertainties (and their covariances) are calculated by the least squares method described in 0. In this case, the variables, x_i and y_i are time series of Julian dates and radiance biases estimated in 6.3 for each orbit since the most recent *trend reset*, respectively.

6.5.3 Infrared GEO-LEO inter-satellite/inter-sensor Class

As above.

6.5.4 Specifics for Operational Meteosat-IASI

As above.

6.6 Generate Plots for GSICS Bias Monitoring

6.6.1 Purpose

The results should be reported quantifying the magnitude of relative biases by inter-calibration. This should allow users to monitor changes in instrument calibration.

6.6.2 General Options

Plots and tables of relative biases and uncertainties for standard radiances should be produced. These may show the evolution of the biases and their dependence on geophysical variables. These all results should be uploaded to the GSICS Data and Products server, and made available from the GPRC's appropriate inter-calibration webpage.

6.6.3 Infrared GEO-LEO inter-satellite/inter-sensor Class

Plots should be regularly updated showing the relative brightness temperature biases for the standard radiances in each channel as time series with uncertainties. The trend line and monthly mean biases (and their uncertainties) should be calculated from these time series, following the example in Figure 13. This allows the most recent result to be tested for consistency with the series of previous results. If significant differences are found operators should be alerted, giving them the opportunity to investigate further.

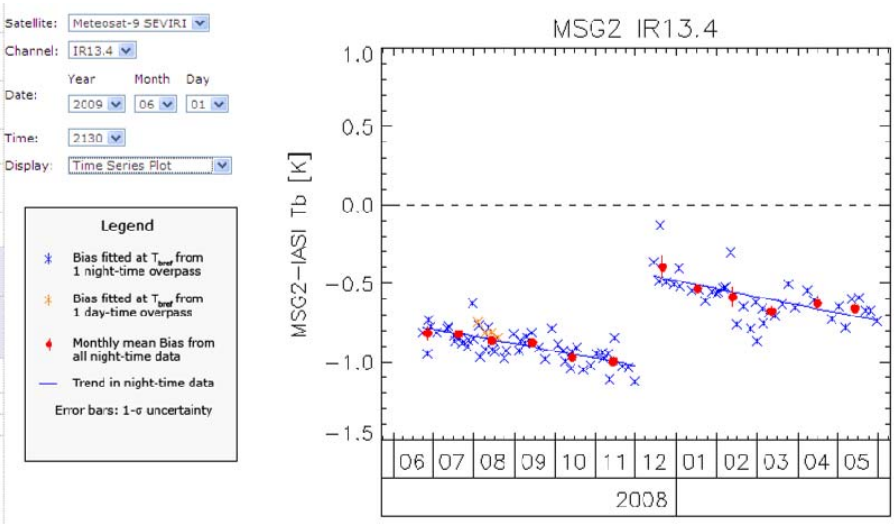

Figure 13: Example of time series plot showing relative bias of IR13.4 channel of Meteosat-9 and IASI at reference radiance following inset legend.

6.6.4 Specifics for Operational Meteosat-IASI

The GSICS Bias Monitoring plots are now generated separately using a dedicated tool, which reads data directly from the netCDF files containing the GSICS Corrections. So this step is only needed for internal monitoring.

7 FLOW SUMMARY OF STEPS 5 AND 6 FOR SEVIRI-IASI

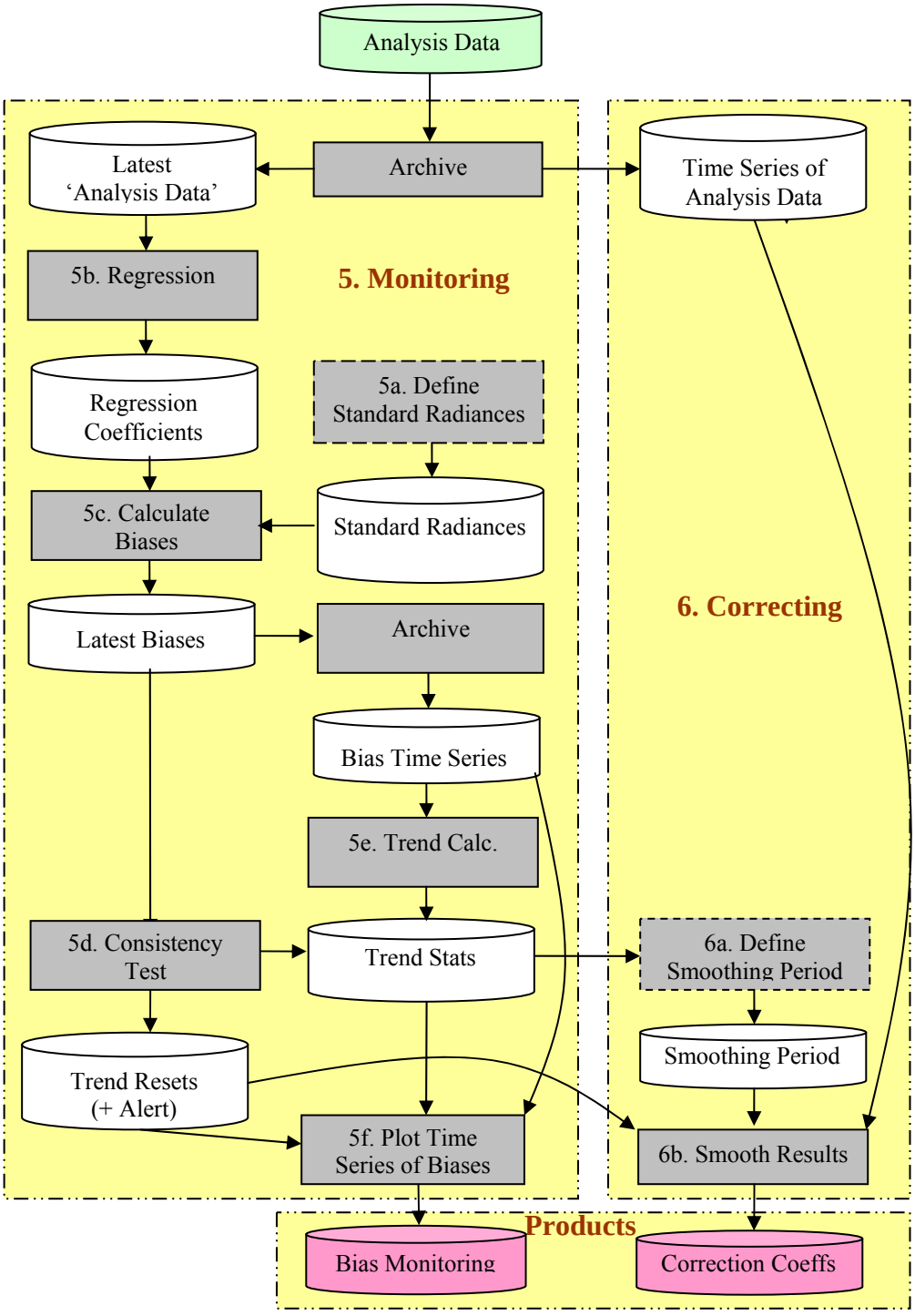

Figure 14: Summary of Recommended Data Flow within Steps 5 and 6 for SEVIRI-IASI

8 GSICS CORRECTION

This final step of the systematic algorithm is to calculate the GSICS Correction, allowing the calibration of one instrument's observed data to be modified to become consistent with that of the reference instrument. The form of the GSICS Correction will be defined offline and can be instrument specific. However, application of the correction relies on the *Correction Coefficients* supplied by the inter-comparisons performed in the previous steps of the algorithm from the *Analysis Data*.

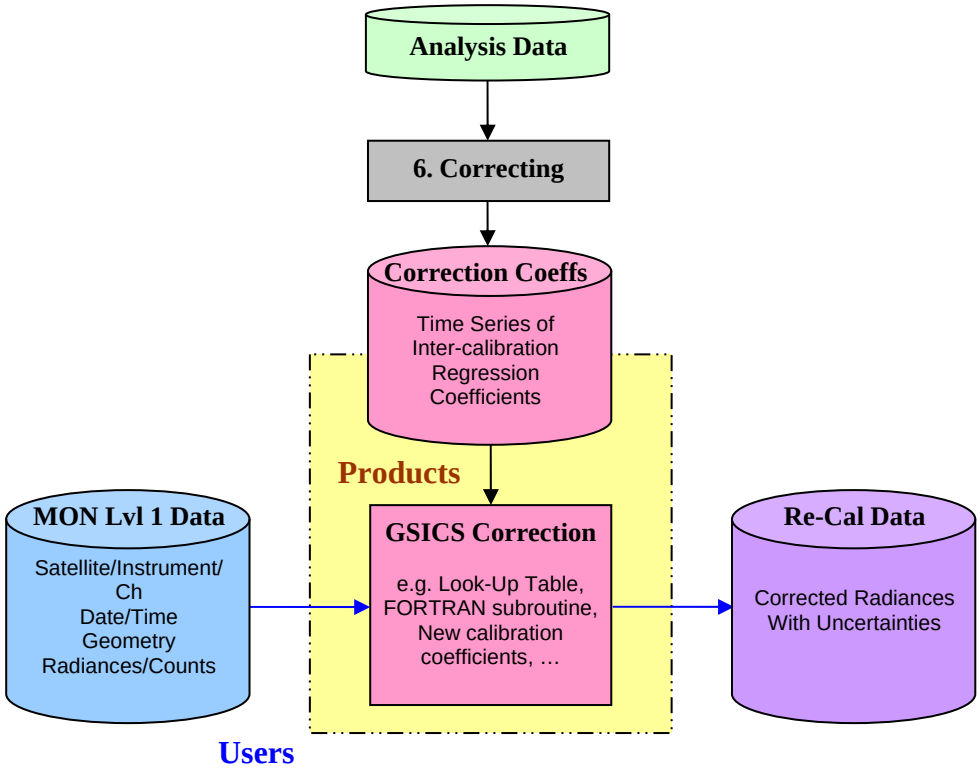

Figure 15: Step 6 of Generic Data Flow, showing inputs and outputs, and illustrating schematically how the correction could be applied by users.

8.1 Define Smoothing Period (Offline)

8.1.1 Purpose

It is possible to combine data from a time series of inter-comparison results to reduce the random component of the uncertainty on the final GSICS Correction. (See 8.1). However, this requires us to define representative periods over which the results can be smoothed without introducing bias due to calibration drifts during the smoothing period. This period can be defined by comparing the observed rate of change of inter-comparison results with a pre-determined threshold, based on the required or achievable accuracy. In general, this definition is performed offline as it requires an in-depth analysis of the instruments' relative biases and consideration of likely explanatory mechanisms. However, it could also be fine-tuned in near real-time. The following describes the general approaches that should be implemented.

8.1.2 General Options

In 6.5.2, time series of radiance biases are regressed against date as the independent variable. This yields an estimate of the rate of change of bias with time, $\frac{d\Delta\hat{y}_{REF}}{dt}$, which can be compared to the threshold Δy_{max} to determine the smoothing period, τ_s:

Equation 21: $\tau_s = \Delta y_{\max}\left(\frac{d\Delta\hat{y}_{REF}}{dt}\right)^{-1}$

8.1.3 Infrared GEO-LEO inter-satellite/inter-sensor Class

As above.

8.1.4 Specifics for Operational Meteosat-IASI

As above.

8.1.4.1 Specifics for Prototype MVIRI-IASI

The threshold value is taken to correspond to the typical uncertainty on the inter-comparison, which is equivalent to $\Delta y_{max} \equiv 0.1$ K.

The MVIRI channel with the highest rate of change is IR-1,
where $\frac{d\Delta\hat{y}_{REF}}{dt} \approx -0.1K/month$.

This yields the following smoothing periods:

$\tau_s \approx 14.5$ days for the Near Real-Time Correction
$\tau_s \approx 29$ days for the Near Real-Time Correction (to match the orbital repeat cycle of Metop)

8.1.4.2 Specifics for Operational SEVIRI-IASI

As above, where the threshold value is taken to correspond to the typical uncertainty on the daily inter-comparisons, which is equivalent to $\Delta y_{max} \equiv 0.05$ K.

The SEVIRI channel with the highest rate of change is IR13.4,
where $\frac{d\Delta\hat{y}_{REF}}{dt} \approx -0.05\ K/month$.
This yields the following smoothing periods:
$\tau_s \approx 14.5$ days for the Near Real-Time Correction
$\tau_s \approx 29$ days for the Near Real-Time Correction (to match the orbital repeat cycle of Metop)

8.2 Calculate Coefficients for GSICS Near-Real-Time Correction

8.2.1 Purpose

In order to reduce the random component of the uncertainty on the GSICS Correction, it is necessary to combine data from a time series of inter-comparison. The regression process described in 6.2 is repeated using all the collocated radiances obtained over the smoothing period defined in 8.1. The resulting regression coefficients (and uncertainties) provide the *Correction Coefficients* used as input to the GSICS Correction. These regression coefficients are then used to evaluate the *Standard Bias* (also with uncertainties) at a set of *Standard Radiances*. The correction coefficients and standard biases are supplied in a netCDF format [defined at https://cs.star.nesdis.noaa.gov/GSICS/NetcdfConvention].

8.2.2 General Options

All the collocation data within the smoothing period before and including the current date is combined and the regression of 6.2 repeated on the aggregate dataset. This approach ensures all data is used optimally, with appropriate weighting according to its estimated uncertainty.

8.2.3 Infrared GEO-LEO inter-satellite/inter-sensor Class

As above.

8.2.4 Specifics for Operational Meteosat-IASI

Implement as above, using a smoothing period *t*-14d to *t*-0 (where *t* is the current date).

8.3 Calculate Coefficients for GSICS Re-Analysis Correction

8.3.1 Purpose

In order to reduce the random component of the uncertainty on the GSICS Correction, it is necessary to combine data from a time series of inter-comparison. The regression process described in 6.2 is repeated using all the collocated radiances obtained over the smoothing period defined in 8.1. The resulting regression coefficients (and uncertainties) provide the *Correction Coefficients* used as input to the GSICS Correction. These regression coefficients are then used to evaluate the *Standard Bias* (also with uncertainties) at a set of *Standard Radiances*. The correction coefficients and standard biases are supplied in a netCDF format [defined at https://cs.star.nesdis.noaa.gov/GSICS/NetcdfConvention].

However, because the smoothing period for the Re-Analysis Correction is defined to be symmetric about the validity date of the GSICS Correction coefficients, it is necessary to perform this step after a correspond delay of at least half the smoothing period after the validity date.

8.3.2 General Options

All the collocation data within the smoothing period before and including the current date is combined and the regression of 6.2 repeated on the aggregate dataset. This approach ensures all data is used optimally, with appropriate weighting according to its estimated uncertainty. This is the recommended approach in general for GSICS.

8.3.3 Infrared GEO-LEO inter-satellite/inter-sensor Class

As above.

8.3.4 Specifics for Operational Meteosat-IASI

As above, using a smoothing period t-14d to t+14 (where t is the validity date).

8.4 Re-Calculate Calibration Coefficients

8.4.1 Purpose

This component aims to produce revised sets of calibration coefficients for one instrument following its inter-calibration against a reference instrument using the *Analysis Data* provided by Step 4. These would allow users to recalibrate data from the monitored instrument to be consistent with the reference instrument. Tables of recalibration coefficients for near-real-time and archive data should also be produced.

8.4.2 General Options

The regression coefficients provided as the *Analysis Data* output from Step 4 are transformed to generate new *correction coefficients* (together with estimates of their uncertainties as full covariances). These can then be used to convert the observations of the monitored instrument into radiances consistent with the GSICS reference standard.

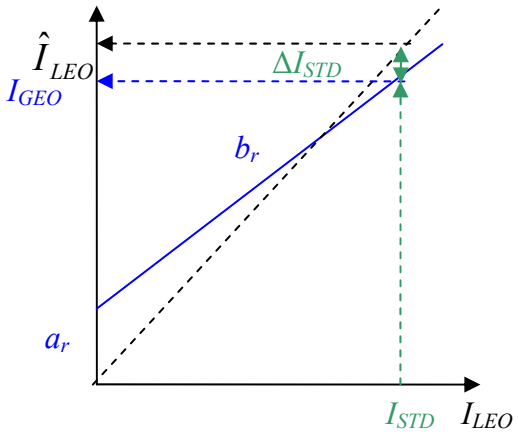

Figure 16: Relationship between radiances observed by geostationary instrument,* $\mathbf{I_{GEO}}$ *and those observed by reference instrument in low Earth orbit,* $\mathbf{I_{LEO}}$*, showing relative bias for standard radiance,* $\mathbf{I_{STD}}$*.

8.4.3 Infrared GEO-LEO inter-satellite/inter-sensor Class

The regression of the aggregated collocated radiances in 8.2 and 8.3 yields estimates of the coefficients, a_r and b_r, required to convert GEO radiances, I_{GEO}, to the reference LEO radiances, I_{LEO}:

Equation 22: $I_{GEO} = a_r + b_r I_{LEO}$

This relationship can be inverted to apply the regression coefficients, a_r and b_r, to convert GEO radiances, I_{GEO}, into radiances consistent with the LEO reference instrument, $\hat{I}_{LEO}$,

Equation 23: $\hat{I}_{LEO} = -\frac{a_r}{b_r} + \frac{1}{b_r} I_{GEO}$,

together with the estimated uncertainty:

Equation 24: $\sigma^2_{\hat{I}_{LEO}} = \left(\frac{\sigma_{a_r}}{b_r}\right)^2 + \left[(I_{GEO} - a_r)\sigma_{b_r}\right]^2 - 2\frac{(I_{GEO} - a_r)}{b_r}\sigma_{a_r b_r}$,

8.4.4 Specifics for Operational SEVIRI-IASI

For SEVIRI, we can also implement a variation of 0 above. Because SEVIRI's level 1.5 counts are linear with radiance and the calibration coefficients used to convert between the units are constant, we can express the GSICS Correction in terms of modified calibration coefficients. In this case, the regression coefficient, a_r and b_r, (and their uncertainties) can be compared with the original calibration coefficients required to convert GEO counts, C_{GEO}, into radiances, I_{GEO}:

Equation 25: $I_{GEO} = a_c + b_c C_{GEO}$

Comparing the two equations above, yields the relationship between the GEO counts and the equivalent radiance of the reference instrument, $\hat{I}_{LEO}$:

Equation 26: $\hat{I}_{LEO} = a_g + b_g C_{GEO}$, where $a_g = \frac{a_c - a_r}{b_r}$ and $b_g = \frac{b_c}{b_r}$.

where a_g and b_g are new calibration coefficients (with uncertainties) which convert GEO counts, C_{GEO}, into radiances consistent with the LEO reference instrument, $\hat{I}_{LEO}$, together with the estimated uncertainty:

Equation 27: $\sigma^2_{\hat{I}_{LEO}} = \left(\frac{\sigma_{a_r}}{b_r}\right)^2 + \left[(a_c - a_r + b_c C_{GEO})\sigma_{b_r}\right]^2 + 2\frac{(a_c - a_r + b_c C_{GEO})}{b_r^3}\sigma_{a_r b_r}$.

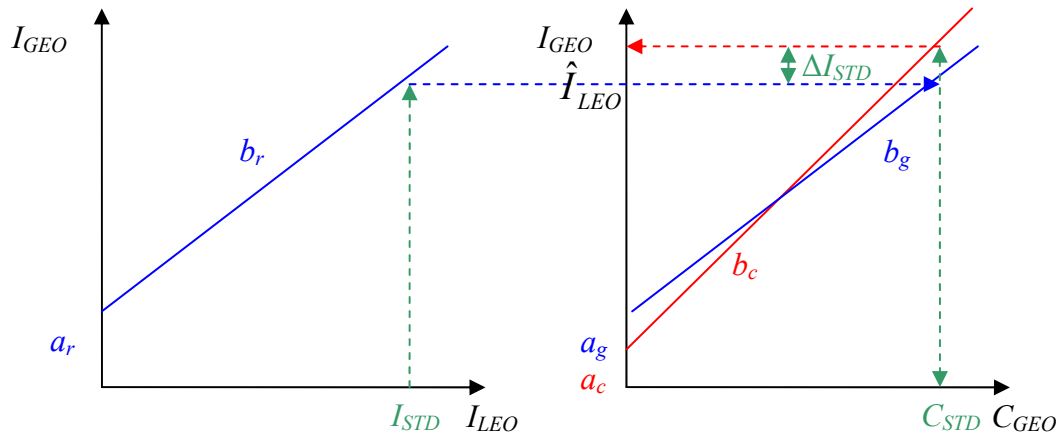

Figure 17: Left panel shows relationship between radiances observed by geostationary instrument, I_{GEO} and those observed by reference instrument in low Earth orbit, I_{LEO}. Right panel shows relationships between the level 1.5 counts and the radiances calculated using the original calibration coefficients (in red) and using the GSICS Corrected coefficients (in blue). The relative bias for standard radiance, I_{STD} is also shown in green.

9 DIAGNOSING

The flow diagram shown in Figure 1 includes an important step, which is not part of the formal algorithm – that of diagnosing the route-cause of the observed biases. This process cannot be automated, so is not formally described in this ATBD. However, it involves expert analysis of the results of the inter-calibration to gain insight into the underlying causes and reporting these. This should be accompanied by recommendations to modify operational practices to reduce the observed biases – e.g. modifying spectral response functions, making specific improvements to future instrument design and/or pre-launch characterisation, etc. These analysis and recommendations take the form of written reports, which themselves may be considered as GSICS deliverables, and represent the final benefit of GSICS.

References

Clough, S. A., and M. J. Iacono, 1995: Line-by-line calculations of atmospheric fluxes and cooling rates II: Application to carbon dioxide, ozone, methane, nitrous oxide, and the halocarbons. J. Geophys. Res., 100. 16519-16535.

EUMETSAT, 2005: Meteosat Normalised Spectral Responses Meteosat-7, http://www.eumetsat.int/website/wcm/idc/idcplg?IdcService=GET_FILE&dDocName=PDF_TEN_SPECTR-RESP-MET-7&RevisionSelectionMethod=LatestReleased&Rendition=Web

EUMETSAT, 2006: MSG SEVIRI Spectral Response Characterisation, EUM/MSG/TEN/06/0010.

EUMETSAT, 2007: Typical Radiometric Accuracy and Noise for MSG-1/2, EUM/OPS/TEN/07/0314.

EUMETSAT, 2008: IASI Level 1 Products Guide, Ref.: EUM/OPS-EPS/MAN/04/0032, http://oiswww.eumetsat.org/WEBOPS/eps-pg/IASI-L1/IASIL1-PG-4ProdOverview.htm#TOC411

EUMETSAT, 2010: GSICS SEVIRI-IASI Inter-calibration Uncertainty Analysis, EUM/MET/TEN/09/0668.

EUMETSAT, 2011: Report on trial relaxation of GSICS geometric collocation threshold, EUM/MET/REP/11/0263.

EUMETSAT, 2012: The Conversion from Effective Radiances to Equivalent Brightness Temperatures EUM/MET/TEN/11/0569.

EUMETSAT, 2015: User Guide for EUMETSAT GSICS Corrections for inter-calibration of Meteosat-SEVIRI with Metop-IASI, EUM/TSS/MAN/15/803180.

Hewison, T.J., 2009: Quantifying the Impact of Scene Variability on Inter-Calibration, GSICS Quarterly, Vol. 3, No. 2, 2009.

Hewison, T.J, 2013: An Evaluation of the Uncertainty of the GSICS SEVIRI-IASI Inter-Calibration Products, *IEEE Trans. Geosci. Remote Sens*., vol. 51, no. 3, Mar. 2013, doi:10.1109/TGRS.2012.2236330.

Minnis, P., A. V. Gambheer, and D. R. Doelling, 2004: Azimuthal anisotropy of longwave and infrared window radiances from CERES TRMM and Terra data. *J. Geophys. Res.*, **109**, D08202, doi:10.1029/2003JD004471.

Press, W.H., S.Teukolksy, W.T. Vetterling and B. Flannery, 1992: Numerical recipes in FORTRAN 77: the art of scientific computing, Second edition, Cambridge University Press.

Rothman et al., 2003: The HITRAN molecular spectroscopic database: edition of 2000 including updates through 2001, Journal of Quantitative Spectroscopy and Radiative Transfer. vol. 82, 5-44.

Schmetz, J. *et al.*, 2002: An Introduction to Meteosat Second Generation (MSG) – and supplements, *Bull. Amer. Meteor. Soc.*, **83**, 977–992, doi:10.1175/1520-0477(2002)083<0977:AITMSG>2.3.CO;2, http://dx.doi.org/10.1175/BAMS-83-7-Schmetz-1.

Tahara, Yoshihiko and Koji Kato, 2009: New Spectral Compensation Method for Intercalibration Using High Spectral Resolution Sounder, Meteorological Satellite Center Technical Note, No. 52, 1-37.

Tjemkes, S.A., 2005: On the conversion from radiance to equivalent brightness temperature, http://cimss.ssec.wisc.edu/~mpav/pdf_msg_seviri_rad2bright.pdf

Wu, X., 2009: GSICS GOES-AIRS Inter-Calibration Algorithm at NOAA GPRC, Draft version dated January 5, 2009.